This paper appeared in CHAOS **3**, 215 (1993).

Attractor Vicinity Decay for a Cellular Automaton

James P. Crutchfield
James E. Hanson

Center for Complex Systems Research
Beckman Institute for Advanced Science and Technology
University of Illinois
405 North Mathews Avenue
Urbana, Illinois 61801*

Abstract

We study the temporal decay of an attractor's vicinity for a domain-wall dominated cellular automaton (CA). Using selected initial pattern ensembles, state space structures in this high-dimensional nonlinear spatial system can be identified via the resulting decay to its attractors. Considered over a range of lattice sizes, the decay behavior falls into three main classes, each of which shows a characteristic profile. The first consists of even-size lattices showing a decelerating decay to small nonattracted ensemble fractions. The second class, also for even lattices, is a catastrophic decay to very small or vanishing nonattracted fractions. The third class also shows catastrophic decay and contains all odd-size lattices. Stochastic models are constructed that mimic the behavior of typical lattices throughout their evolution until finite-size effects appear. Weak additive noise causes all states on all lattices to fall into the attractor. In the end we find it overwhelmingly likely that the recently-proposed attractor-basin portrait captures the CA's qualitative dynamics.

*Permanent address: Department of Physics, University of California, Berkeley CA 94720 USA; JPC's Internet address is chaos@gojira.berkeley.edu; JEH's is hanson@gojira.berkeley.edu.

Contents

1 State Space Geometry and Relaxation Processes

The state space geometry of large spatial systems is impossible to directly analyze since the dimension is far too high. Some method of projecting onto a space of lower dimension is needed. Existing indirect techniques usually expand with respect to some spatially global pattern function basis, such as Fourier or normal modes.[1–3] These methods are appropriate when there is strong spatial coherence. Localized function bases, such as solitons, can be used for expansion even if spatial coherence is lacking, assuming one knows in advance the appropriate functional form for the solitons.[4,5] Roughly speaking, the state space geometry in these cases consists of nested tori whose local coordinates describe the relative phase information of the solitons' motion. An alternative approach for studying high-dimensional state spaces is to design initial condition ensembles that probe subspace structures controlling relaxation dynamics.[6] Notably, this is independent of the presence or absence of spatial coherence. In the following we apply this method to a very simple class of spatial systems, cellular automata (CA).[7] The particular example analyzed exhibits strong spatial decorrelation, but is nonetheless highly structured, with spatial patterns consisting of chaotic domains separated by diffusing walls.

In an attempt to capture the state space geometry of high-dimensional systems, we recently proposed a computation theoretic framework for investigating the qualitative dynamics of extended systems. The attractor-basin portrait of a cellular automaton was given in terms of formal languages that described pattern ensembles.[8] Continuing in this vein we investigate here various decay processes revealed by the relaxation of selected initial pattern ensembles. The focus is on the statistical properties that control the stability of the CA's regular attractors. The primary goal in this and in a companion work is to quantitatively demonstrate that exceptions to the attractor-basin portrait analysis, though inevitably present, represent a vanishingly small fraction of initial conditions and lattice sizes. A secondary motivation is to address several of the simpler issues that will arise in the future development of techniques for identifying state space structures in high-dimensional nonlinear spatial systems.

2 Cellular Automata

Many CA exhibit "domains" of homogeneous spatio-temporal structure that are separated by "walls". In the following we take the nearest-neighbor elementary CA (ECA) rule 18 as an exemplar of this large class. It is arguably the simplest nonlinear CA. The neighborhood patterns $\{001, 100\}$ at time t map to a center cell of value 1 at time $t+1$; all others map to 0. Unlike other chaotic CA such as ECA rule 90, ECA 18 does not obey a linear superposition principle. This is the sense in which it is nonlinear.

The domains of ECA 18 have a simple property: every other cell is 0. Between those sites are "wild-card" sites that can be either 0 or 1. Its walls break this spatial symmetry with a pattern of $1(00)^n1, n = 0, 1, 2, \ldots$, which places a 1 on a site that, if it were in a domain, should have a 0. Thus, for example, two consecutive 1s separate two domains: one domain has 0s on even sites; the other, 0s on odd sites. We refer to these walls as dislocations. Figure 1 shows the temporal evolution of ECA 18 dislocations starting from an arbitrary initial pattern using a "filtered" space-time diagram that factors out the intervening chaotic domains.

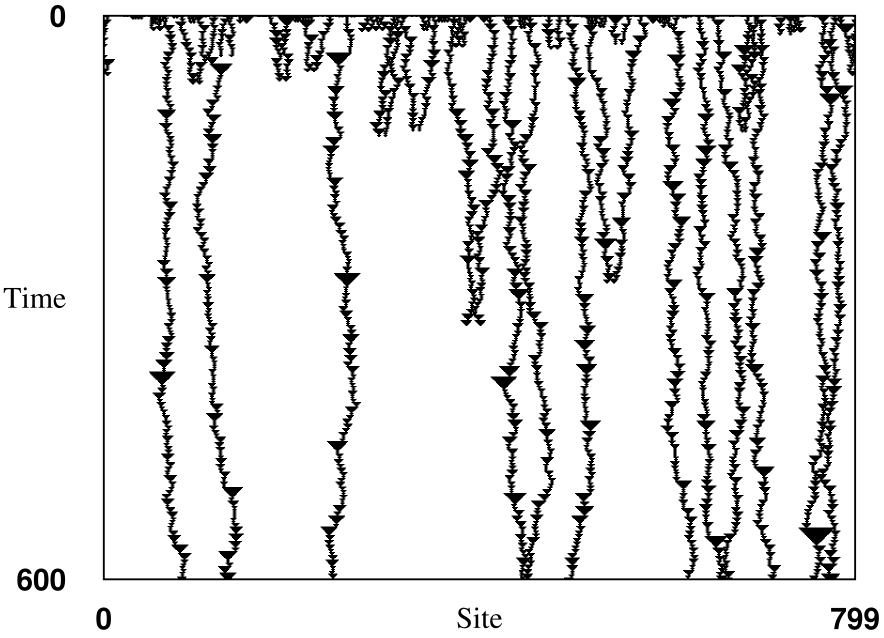

Fig. 1. The temporal evolution of dislocations $1(00)^n1$ under elementary cellular automaton 18, starting from an arbitrary initial pattern. The diagram was produced using spatial transducers from Ref. [8]. The chaotic domains have been factored out leaving the dislocations highlighted.

The dislocations appear to move randomly: At each time step they must move either left or right, the choice being determined (ultimately) by bits in the initial condition. When two dislocations are sufficiently near they can annihilate by merging into a $10(00)^n1$ pattern, a nonlinear and irreversible process. It gives rise to the apparent nonlocal annihilation seen, for example, near the center of Fig. 1. Starting from an arbitrary initial pattern ECA 18 appears as a gas of randomly diffusing, annihilating dislocations superposed on a chaotic background.[9] The motion of a single dislocation between two semi-infinite (random) domains recently was shown to obey a random walk.[10] Similar results for two or more dislocations are substantially more difficult to obtain since the dislocations' motion eventually becomes correlated due to the overlap of their reverse-time light-cones. This difficulty lies at the root of the problem we investigate here and is one reason the semi-empirical approach we take is a necessary complement at this time to the rigorous analysis.

An algebraic analysis of CA has recently begun to address some of the robust properties due to nonlinearity and strong dislocation interactions. For example, it has been shown that ECA 18 patterns with dislocations can be linearized.[11] The algebraic techniques describe much of the combinatorial structure of the discrete state space of CA on finite lattices. The number and type of periodic orbits for ECA 18 on a given lattice size can be determined, for example.[12] Not surprisingly, the detailed behavior is highly sensitive to the number-theoretic properties of the lattice size N, such as its prime factorization. This leads to large fluctuations in the calculable properties as a function of lattice size that can obscure common features of the CA's behavior.

3 Qualitative Dynamics

The qualitative dynamics of a dynamical system is the description of the state space in terms of attractors, basins, and separatrices.[13,14] This gives a picture of the global architecture of state space, without attempting to find closed-form solutions of an individual pattern's evolution. The discreteness of CA state space and the spatial nature of CA pose a number of problems for this type of analysis. Nonetheless, a general procedure for constructing attractor-basin portraits of CA that overcomes many of the problems has recently been developed and applied to the particular case of ECA 18 [8] and to a wide range of other CA.[15]

One useful feature of this qualitative analysis is that it traces the development of spatial patterns arising in the CA states, rather than following the exact evolution of any single configuration. This allows for a qualitative characterization of the typical behavior of the system, avoiding the proliferation of details involved in tracking individual trajectories. In addition, it is independent of the particular lattice size and spatial origin. We give a brief synopsis of the results for ECA 18 here.

One view of ECA 18's attractor-basin portrait is shown in Fig. 2. Each symbol in the figure corresponds to an ensemble of CA states with specific properties. On finite, periodic lattices of even size N, only the portion of the figure to the left of the left dashed line is present. For finite odd N, the portion to the right of the right dashed line exists. On infinite lattices, the entire figure is present. At the bottom of the figure are the two attractors, Λ^0 and $\Lambda^{0,0}$. These ensembles are temporally invariant and stable to perturbations. Λ^0 consists of states with no dislocations; $\Lambda^{0,0}$ is made up of states with a single dislocation due to the odd lattice size. The possible effects of small perturbations $\delta\Lambda$ on states in Λ^0 and $\Lambda^{0,0}$ are shown by the thin curving lines. The basins of the attractors, B^0 and $B^{0,0}$, represent the sets of CA states that evolve to some state in Λ^0 and $\Lambda^{0,0}$, respectively. The global separatrix S breaks up into subseparatrices S_{even}, S_{odd}, and S_∞. Finally, A^N, with $A = \{0, 1\}$, is the set of all CA states on the lattice.

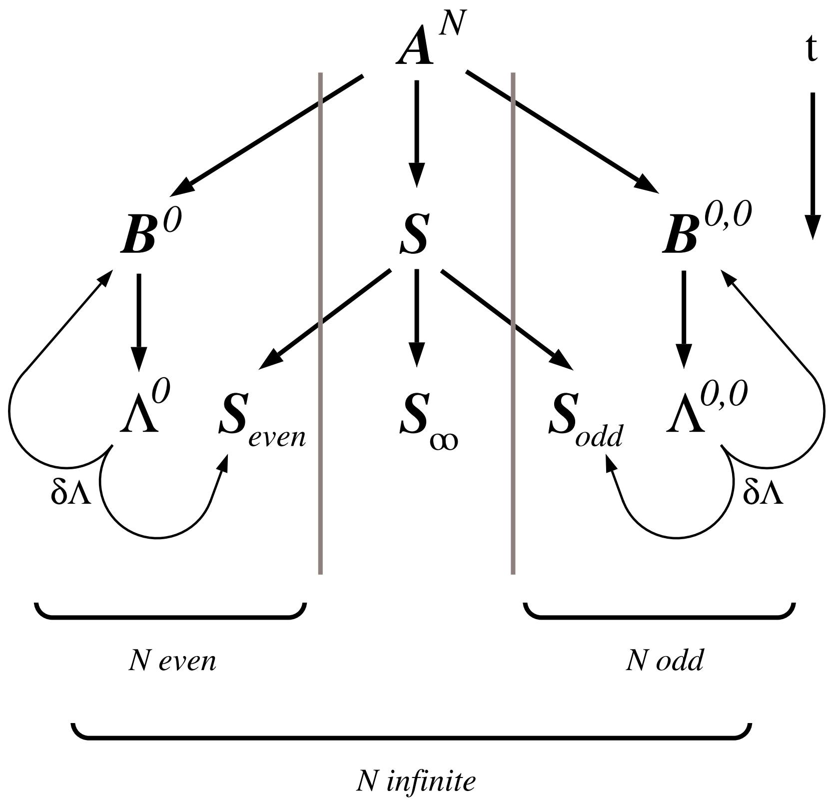

Fig. 2. A skeletal picture of rule 18's attractor-basin portrait. The view is that in process language space and includes both finite odd and even lattices along with infinite lattices. The various symbols indicate the formal languages identified in the computation theoretic analysis of Ref. [8]. The temporal evolution from one language to another goes down the page. The thin lines with arrows indicate the effect of perturbations $\delta\Lambda$ away from the attractors. Figure reproduced from Ref. [8].

4 Vicinity Convergence

The stability of the attractor under small perturbations is investigated in terms of the attractor's vicinity. Due to the lack of a preferred metric on discrete CA state spaces, there are several alternatives for the vicinity, such as (i) the subbasins b_w with $w = 2$ dislocations on even lattices or $w = 3$ on odd lattices, or (ii) the Hamming vicinity. The latter, in which perturbations are spatially localized bit-flips, is the more physically realistic of the two if one thinks of the bit-flips as being due to thermal fluctuations. Typical states in the b_w-subbasin vicinity require perturbations correlated over long distances. For this reason, we will focus primarily on the Hamming vicinity in the following. The perturbation we consider, arguably the "smallest" one possible, is a single bit-flip somewhere in the state. If the site flipped is not a wild-card site, this perturbation pushes the state off the attractor by generating a pair of dislocations, which then move about on the lattice and ultimately may or may not collide and annihilate. If and when the dislocations annihilate, the state falls back into the attractor.

Under the action of ECA 18 not all of the patterns in this vicinity fall back into the attractor, even asymptotically. Thus, on lattices with even size N, the vicinity V^0 breaks up into two disjoint subsets, determined by the two possible asymptotic $(t \to \infty)$ behaviors: (i) the set E^0 of states that eventually evolve back into the attractor, and (ii) the set P^0 of states that evolve onto temporally periodic orbits not in Λ^0. By definition, $E^0 = B^0 \cap V^0$ and $P^0 = S_{even} \cap V^0$. In Fig. 2, these two possible asymptotic behaviors are indicated by the two curved lines leading away from Λ^0. For N odd, the situation is analogous, with the vicinity $V^{0,0}$ breaking up into $E^{0,0}$ and $P^{0,0}$. In the following we will consider $\{V, \Lambda, E, P\}$ to be $\left\{V^0, \Lambda^0, E^0, P^0\right\}$ for N even, and to be $\left\{V^{0,0}, \Lambda^{0,0}, E^{0,0}, P^{0,0}\right\}$ for N odd.

The states in the Hamming vicinity are generated by a two step process. First, a state is produced using the appropriate attractor machine.[8] Second, a site is selected at random and its value is set randomly to 0 or 1. With probability $\frac{1}{2}$ this changes the state; the result may or may not be in the attractor. And with probability $\frac{1}{4}$ a pair of dislocations is created, knocking the pattern off the attractor into the vicinity. The resulting interdislocation distance $d > 0$ is distributed exponentially as

$$Pr(d = x) = \begin{cases} 2^{-(x+1)/2}, & x = 1, 3, 5, \ldots \\ 0, & \text{otherwise} \end{cases} \tag{1}$$

An ensemble with M members will have at $t = 0$ approximately $M/4$ patterns off the attractor.

A vicinity ensemble's decay can be monitored by the fraction $f_\Lambda(t)$ of ensemble states on the attractor as a function of time. For a fixed lattice size at a given time, we define the complementary fraction $f_P(t)$ of nonattracted patterns in the vicinity ensemble as

$$f_P(t) = \frac{\|\mathbf{\Phi}_t(V) - \Lambda\|}{\|V\|} \tag{2}$$

where $\mathbf{\Phi}_t(V)$ is the set of time t iterates of all states in the vicinity V under the CA rule, and $\|L\|$ denotes the cardinality of the set L. The set-theoretic difference $\mathbf{\Phi}_t(V) - \Lambda$ denotes the ensemble of states in $\mathbf{\Phi}_t(V)$ not yet on the attractor. Clearly, $f_P(t)$ is monotonically nonincreasing with t, and $f_\Lambda(t) + f_P(t) = 1$. The asymptotic nonattracted fraction is given by

$$f_P = \lim_{t \to \infty} f_P(t) \tag{3}$$

We define the convergence time T_c as the first time-step at which $f_P(t)$ reaches its asymptotic value. Note that on any given finite lattice $f_P = \|P\| / \|V\|$, the fraction of vicinity states evolving to periodic orbits not in the attractor.

The decay profile $f_P(t)$ gives an indirect indication of the orbit structure of the high-dimensional state space. On a finite lattice with periodic boundary conditions, all states eventually fall onto temporally periodic orbits. In particular, starting from any given initial state s_0 in the vicinity V, the trajectory $\{s_1, s_2, s_3, ...\}$ will at some point fall onto a periodic orbit either in the attractor Λ or in the nonattracted set P. If this orbit is in Λ, then there is a time τ at which it first fell into Λ. We therefore define a transient starting in V as a sequence of states $\{s_0, s_1, ..., s_{\tau-1}\}$ such that (i) the initial state s_0 lies in the vicinity, (ii) the last state $s_{\tau-1}$ is not in the attractor, and (iii) the iterate $s_\tau = \Phi(s_{\tau-1})$ of the last state is in the attractor. Note that this definition excludes states in P. All states on transients starting in the Hamming vicinity have two dislocations if N is even, or three dislocations if N is odd. The transient length τ is equal to the number of states in that part of the trajectory that lies outside Λ. The fraction of states in the ensemble with transient length τ is given by the instantaneous decay rate

$$\Delta f_P(\tau) \equiv f_P(\tau) - f_P(\tau - 1) \tag{4}$$

In this way, the decay curve $f_P(t)$ is the integral of the transient-length probability density. Furthermore, since $f_P(t)$ can change only while there are states on transients, T_c is equal to the length of the longest transient. What $f_P(t)$ fails to capture is the detailed architecture of the state space, i.e., the connectivity of the trajectories.

5 Random Cliff Walkers

In ECA 18, the final decay of an arbitrary initial pattern to the attractor usually reduces to the annihilation of only two dislocations. On an even lattice two dislocations collide leaving a pattern on the attractor Λ^0 with none; on an odd lattice two of three collide leaving a pattern on $\Lambda^{0,0}$ with one dislocation. The stochastic analog of the net process is that the dislocations diffuse according to a random walk and two of them eventually annihilate when their paths cross. The question in this view becomes whether ECA 18 with patterns restricted to the vicinity behaves effectively like a stochastic process.

A crude approximation of dislocation evolution, valid in the limit of vanishing dislocation density, was given in Ref. [8]. That probabilistic model is inadequate for Hamming vicinity decay since, as just noted in Eq. (1), the dislocation density is weighted toward small separations. As an alternative, we now describe the random cliff walker (RCW), a simple stochastic process that captures the basic phenomenon. The RCW model, and modifications described below, are variants of a random walk with absorbing barriers.[16,17]

In an ideal random walk a particle moves left or right with equal probability. The distance $d(t)$ between two such particles either stays the same or changes with equal probability. If the distance changes then it is increased or decreased by two units, again with equal probability. In the RCW process two particles annihilate whenever the distance passes through zero. $d(t)$ itself can be considered as a quasiparticle obeying a random walk on the half-line $d > 0$. In effect, there is a cliff at the origin: When dislocations annihilate, d passes through zero and the quasiparticle falls off a cliff. This is modeled by stopping the evolution of $d(t)$ at that point, effectively removing one pattern from the ensemble. The rule for the RCW stochastic process is given by

$$d(t) = d(t-1) + \delta \tag{5}$$

where δ is a random variable with the probability distribution given in Table I. The lattice constant has been changed to $\frac{1}{2}$ so that the possible displacements are $\delta \in \{-1, 0, +1\}$. For convenience, we allow $d(t)$ to take on negative values, but require that quasiparticles with $d(t) \leq 0$ be frozen in place.

Random Cliff Walker	$d(t-1) \leq 0$	$d(t-1) > 0$
$Pr(\delta = +1)$	0	$1/4$
$Pr(\delta = 0)$	1	$1/2$
$Pr(\delta = -1)$	0	$1/4$

Table I. Stochastic evolution of the random cliff walker. The distance between particles evolves according to $d(t) = d(t-1)+\delta$.

Hamming-vicinity decay is simulated by generating an ensemble of M RCW quasiparticles with an exponential distribution like that for the Hamming vicinity [Eq. (1)], namely

$$Pr(d(0) = x) = \begin{cases} 2^{-x-1}, & x \geq 0 \\ 0, & x < 0 \end{cases} \tag{6}$$

The fraction $f_{RCW}(t)$ of surviving particles, i.e. those particles i with $d_i(t) > 0$, is estimated using the statistic

$$f_{RCW}(t) = M^{-1} \sum_{i=0}^{M-1} \Theta_i(t), \text{ where } \Theta_i(t) = \begin{cases} 1 & d_i(t) > 0 \\ 0 & d_i(t) \leq 0 \end{cases} \tag{7}$$

A log-log plot of $f_{RCW}(t)$ vs. t is shown as the solid line in Fig. 3. In this and all succeeding plots, the logarithms are base 2. The curve was computed numerically using an ensemble of $M = 10,000$ particles. The curve is of the form $f_{RCW}(t) = f_{RCW}(1) \cdot t^{-\alpha(t)}$ with $\alpha(t) \to \frac{1}{2}$ from below as $t \to \infty$. For finite time, $\alpha(t) < \frac{1}{2}$, so that $f_{RCW}(t)$ shows a slowly downward curving "backbone" whose slope approaches $-\frac{1}{2}$ as $t \to \infty$. A phenomenological model that gives a reasonable summary of $f_{RCW}(t)$ uses $\alpha(t) = \frac{1}{2}(1 - at^{-b})$ with $a = 0.8$, $b = 0.15$, and $f_{RCW}(1) = 0.22$.

The $\alpha(t) \to \frac{1}{2}$ convergence can be readily understood. An initial RCW ensemble equivalent to dislocation pairs all starting at the same separation $d(0) = 1$ decays like $f_{RCW}(t) \propto t^{-\alpha}$ with $\alpha \approx \frac{1}{2}$ for all t. The form of $f_{RCW}(t)$ observed for the exponentially distributed vicinity

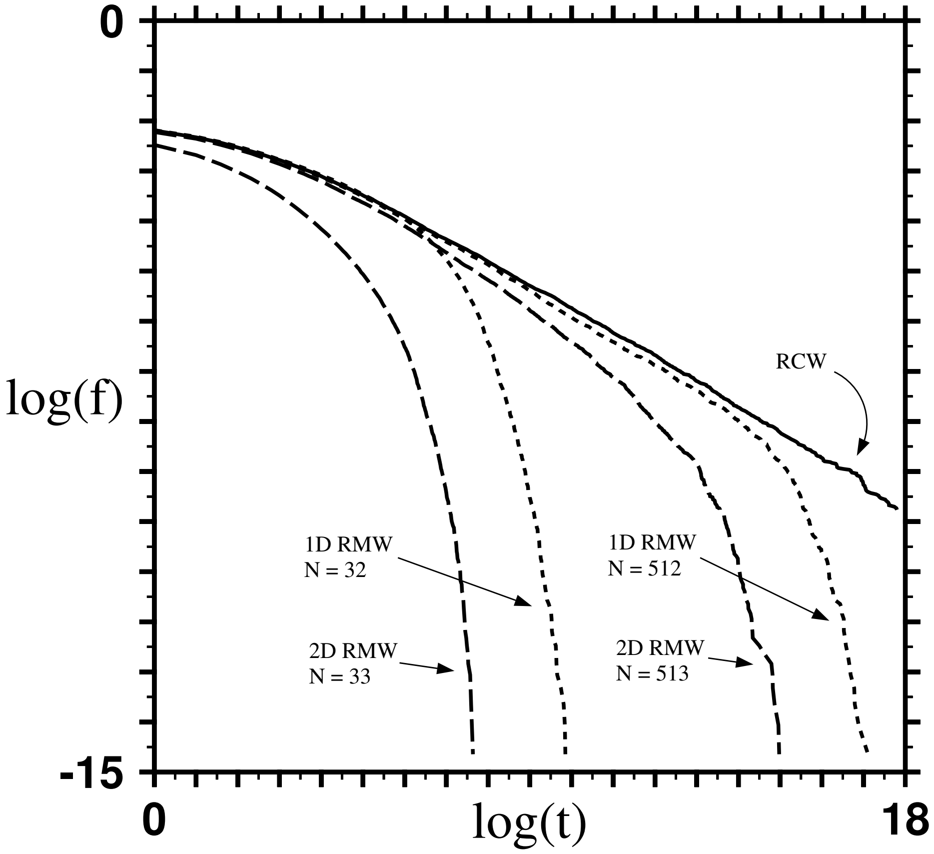

Fig. 3. Decay profiles for annihilating random walks. The random cliff walker decay profile $f_{RCW}(t)$ is the solid line. 1D and 2D random mesa walker profiles $f_{RMW}(t)$ are shown for lattices $N \in \{32, 512\}$ and $N \in \{33, 513\}$, respectively. In this and all succeeding plots, logarithms are base 2. The simulations were performed with ensembles of size $M = 10,000$ for the RCW profile and $M = 12,800$ for each of the RMW profiles.

ensemble is roughly a superposition of the individual decays shifted by the time it takes for the particles to first begin annihilating; the latter is a function of the initial dislocation separation. And so, the decay profile slope gradually decreases to $\alpha = \frac{1}{2}$.

As described, the initial fraction of "active" RCW pairs is $f_{RCW}(0) = \frac{1}{2}$, whereas the initial fraction of ECA 18 dislocations is $f_P(0) = \frac{1}{4}$. This is due to the fact that an ECA 18 state is perturbed off the attractor with probability $\frac{1}{2}$, and so only half of the states in the vicinity ensemble ever participate in the simulation. This is only a difference in normalization, and is corrected in all of the figures.

In comparing the stochastic model to ECA 18, we will be considering the evolution of dislocations on finite lattices with periodic boundary conditions. For even-size lattices, there are two dislocations, which may annihilate either by approaching each other or by diverging from each other until they wrap around the periodic boundary; for odd lattice size, there are three dislocations, any two of which may annihilate. We treat these two cases as separate modifications of the RCW model. A general model, applicable to any number of dislocations, is a straightforward extension. However, since the vicinities we are studying have only two or three dislocations, the general model is unnecessary and is left for development elsewhere.

For two dislocations, the simpler case, we can include the finite-N effects by adding another "cliff" at lattice-site $N/2$ (the factor of $\frac{1}{2}$ comes from the RCW lattice constant, which is $\frac{1}{2}$). The resulting model is a one-dimensional random mesa walker (1D RMW), which has an explicit dependence on the lattice size. The model's one-dimensional nature is emphasized to differentiate it from the two-dimensional random mesa walker developed below. For an exponential distribution of initial dislocation distances $d(0)$ as above, we expect the fraction of surviving dislocations, $f_{RMW}(t)$, to show an early epoch during which it follows $f_{RCW}(t)$, followed by a gradual transition to a second epoch during which $f_{RMW}(t)$ decays at a faster rate. The transition to the second epoch occurs when the random walkers have had sufficient time to reach the second cliff at site $N/2$. Since the root-mean-square excursion $\sigma = \sqrt{\langle d^2 \rangle}$ of a single random walker evolves as $\sigma \propto \sqrt{t}$, the transition time T_d should vary with lattice size as $T_d \propto N^2$.

1D RMW decay profiles $f_{RMW}(t)$ vs. t for lattices $N \in \{32, 512\}$ are plotted on a log-log scale as dotted lines in Fig. 3. For both lattice sizes, the curves were computed numerically using an ensemble of $M = 12,800$ particles. As the figure shows, $f_{RMW}(t)$ follows $f_{RCW}(t)$ up to a deviation time $t \approx T_d$. Numerical experiments on lattices $N \in \left\{2^k : 3 \leq k \leq 9\right\}$ indicated that T_d varies with lattices size as

$$T_d(N) = kN^2, \quad k \approx 0.07 \tag{8}$$

At T_d there is a gradual transition to a faster decay rate. The decay in the second epoch is roughly exponential, with a rate that decreases as N grows larger. In Fig. 3 the transition to the second epoch shows up as a smooth downturn of $f_{RMW}(t)$ away from $f_{RCW}(t)$.

The case with three dislocations, corresponding to ECA 18 on an odd-size lattice, requires a more complex modification, since there are three possible ways for the dislocations to annihilate. We can express the evolution in terms of any two of the three interdislocation distances, i.e., $d_1(t)$ and $d_2(t)$. These move according to the stochastic evolution equation

$$\begin{aligned} d_1(t) &= d_1(t-1) + \delta_1 \\ d_2(t) &= d_2(t-1) + \delta_2 \end{aligned} \tag{9}$$

where δ_1 and δ_2 are random variables with values in $\{-1, 0, +1\}$ and with a joint distribution $p(\delta_1, \delta_2)$ given by

$$\begin{aligned} p(0,0) &= 1/4 \\ p(-1,-1) = p(+1,+1) &= 0 \\ All\ others:\ p(\delta_1, \delta_2) &= 1/8 \end{aligned} \tag{10}$$

The evolution is subject to the constraints

$$\begin{aligned} d_i(t) &> 0, \quad i = 1, 2 \\ d_1(t) + d_2(t) &< (N-1)/2 \end{aligned} \tag{11}$$

Violation of any of these constraints signifies that a pair of random walkers has annihilated, and so evolution stops at that point. In effect, this is a random walk in two dimensions on a triangular mesa, i.e., a 2D RMW on the simplex defined by Eq. (11). The initial distribution corresponding to Hamming-vicinity decay in ECA 18 has $d_1(0)$ distributed exponentially as for the 1D RMW, and $d_2(0)$ uniform over the interval $1 \leq d_2(0) \leq (N-1)/2$. Note that a portion of this distribution lies off the simplex, so that some random walkers are already beyond the edge at time zero; this is the same as for ECA 18.

The dashed lines in Fig. 3 show the 2D RMW decay profiles $f_{RMW}(t)$ vs. t for lattices $N \in \{33, 513\}$. As for the 1D RMW profiles, the curves were computed numerically using an ensemble of $M = 12,800$ particles. The curves do not follow the RCW backbone, but rather start some distance below the backbone and curve smoothly downward. The time-1 fraction $f_{RMW}(1)$ varies with lattice size roughly as

$$f_{RMW}(1) \approx c_1 - c_2/N \tag{12}$$

with $c_1 = 0.22$ and $c_2 = 1.0$. For each N, the 2D RMW decay profile lies below the corresponding 1D RMW curve, indicating a faster decay rate. As for the 1D RMW case, the decay becomes roughly exponential after an initial epoch. The transition to exponential decay sets in earlier and is much more gradual, making a divergence time more difficult to specify. However, the long-time behavior indicates that the transition has the same lattice-size dependence as does the 1D RMW. This can be observed in Fig. 3 by noting that the exponential tails of the 1D and 2D decay profiles for lattices $N \in \{512, 513\}$ are offset by the same amount as for $N \in \{32, 33\}$. Data from lattices $N \in \left\{2^k + 1 : \ 3 \leq k \leq 10\right\}$ indicate that, in the exponential decay epoch, a 2D RMW with lattice size N follows approximately the same curve as a 1D RMW on a lattice of size $N/2$.

If ECA 18 Hamming vicinity decay mimics ideal diffusive annihilation, then its behavior should agree with the 1D RMW stochastic process on even-size lattices, and with the 2D RMW process on odd-size lattices. The temporal decay $f_P(t)$ should follow the same curve as the appropriate $f_{RMW}(t)$. Conversely, deviations from random mesa walker profiles must be ascribed to other decay mechanisms and state space structures than diffusive annihilation on a finite lattice with periodic boundary conditions. As we show in the next section, Hamming vicinity decay of ECA 18 typically mimics the stochastic process quite well throughout most of its evolution.